OPEN ACCESS

University of BRISTOL

Peer reviewed version

University of Bristol - Explore Bristol Research
General rights

Optimal Configurations for a Linear Vibration Suppression Device in a Multi-Storey Building

Sara Ying Zhang[1], Jason Zheng Jiang[1,*,†] and Simon Neild[1]

Department of Mechanical Engineering, University of Bristol, Queen's Building, University Walk, Bristol, BS8 1TR, UK

SUMMARY

This paper investigates the use of a two-terminal vibration suppression device in a building. The use of inerter-spring-damper configurations for a multi-storey building structure is considered. The inerter has been used in Formula 1 racing cars and applications to various systems such as road vehicles have been identified. Several devices that incorporate inerter(s), as well as spring(s) and damper(s), have also been identified for vibration suppression of building structures. These include the tuned inerter damper (TID) and the tuned viscous mass damper (TVMD). In this paper, a three-storey building model with a two-terminal absorber located at the bottom subjected to base excitation is studied. The brace stiffness is also taken into consideration. Four optimum absorber layouts, in terms of how spring, damper and inerter components should be arranged, for minimising the maximum relative displacements of the building are obtained with respect to the inerter's size and the brace stiffness. The corresponding parameter values for the optimum absorber layouts are also presented. Furthermore, a real-life earthquake data is used to show the advantage of proposed absorber configurations. Copyright © 2015 John Wiley & Sons, Ltd.

1. INTRODUCTION

Mitigating the seismic response of a structure has attracted the interest of researchers for many decades. Tuned mass dampers (TMDs) were proposed as a dynamic vibration absorber by Frahm [1] in 1909, then Villaverde [2] and Sadek *et al.* [3] showed that placing the TMDs at the upper stories of buildings is an effective way to reduce the vibrations of the structures. The classical method of choosing the damping ratio is based on the tuning method proposed by Den-Hartog [4] and others [5–8], and Krenk characterised the damping properties of the TMD and identified the optimal damping by analysing the motion of the structural mass as well as the relative motion of the damper mass in [9]. Multiple TMDs [10, 11] and combining TMDs with base-isolation systems [12] have also been shown to be effective in suppressing vibration. The TMDs are widely used as suppression devices for buildings [13–15], however, the downsides of this kind of device are its weight and the fact that the device must be situated of the top of the building for maximum effectiveness. In the early 2000s, Smith [16] introduced a new device, called the 'inerter', which is a two-terminal equivalent to the mass element, with the property that the applied force is proportional to the relative acceleration across its terminals. Applications of inerters in structures have been identified in a wide range of mechanical systems [17–25]. By using inerters for vibration suppression of building structure, the two downsides of the TMD can be eliminated, since the inerter can provide a high inertance with

---

*Correspondence to: Jason Zheng Jiang, Department of Mechanical Engineering, University of Bristol, Queen's Building, University Walk, Bristol, BS8 1TR, UK.
†E-mail:z.jiang@bristol.ac.uk

Prepared using stcauth.cls *[Version: 2010/05/13 v2.00]*

a much lower mass because of it can include significant gearing and the suppression device can be installed at the bottom rather than the top because it generates a force based on the relative motion. In [26], Wang *et al.* identified several simple absorber layouts incorporating inerter device which are beneficial in reducing vibration of a one degree of freedom (DOF) and a two DOF building models. The tuned inerter damper (TID) was proposed in [27] and it has been shown that the performance of a TID mounted across the ground and lowest floor of the structure can be better than that of a TMD mounted at the top of the structure. In [28], Krenk and Høgsberg studied the effect of the other non-resonant modes and proposed a new design method for TMDs and TIDs. Ikago *et al.* [29] presented a new seismic control device the tuned viscous mass damper (TVMD) and analysed the performance of it when installed in a SDOF structure. The TVMD consists of a inerter-like ball screw mechanism mounted in parallel with a viscous damper (which they term as VMD), and a soft spring connecting the VMD to the primary system. This shift spring can be thought of as representing the connecting brace compliance. Comparing with the conventional viscous damper, it also has been shown that the TVMD is the most effective absorber for the single-degree-of-freedom systems with dampers having the same additional damping coefficient. In [30], Ikago *et al.* obtained the optimum response of a MDOF building structure with TVMDs in every story. Inerter-like devices known as inertial dampers have also been introduced in [31]. A new device based on inerter named as TMDI was proposed in [32]. As the inerter has the direct analogy in the electrical domain, the TID has also recently been implemented electrically and coupled to the structure using a coil actuator [33].

In the traditional force-current analogy between mechanical and electrical networks, the physical masses, dampers and springs correspond to the electrical capacitors, resistors and inductors respectively. However, the conventional mass element fails to be fully equivalent to the capacitor, since one terminal of the mass is always connected to the ground. With the invention of the inerter, this problem can be fully solved and the electrical theorems can be directly used in the analysis and synthesis of mechanical networks, thus allows all positive-real mechanical impedances to be synthesised. Both the TID and the TVMD use the inerter in a fixed configuration, which restricts the use of the passive impedances and limits the achievable performance of the mechanical system. In this paper, we use the mechanical admittances to represent the absorber and obtain the optimum configurations of it by the network synthesis theory. Bott-Duffin [34] proposed the most general transformerless synthesis procedure to realise any positive-real functions with a network consisting of resistors, capacitors and inductors. However, this procedure is not ideal since it needs a large number of elements, which is at odds with a mechanical realisation of the device where minimising the network complexity is crucial. By introducing the concept of regularity, Jiang and Smith [35] presented the complete set of biquadratics that can be realised by networks consisting of three resistive and two reactive elements. Applications of biquadratic functions as the mechanical admittances to vehicle suspension have been identified in [17, 23]. It is well known that for the TMD, the mass ratio is very important in civil engineering since adding large mass to the structure imposes additional structural constraints. Due to gearing, the inertance provided by an inerter can far exceed the mass of the device. An effective way to obtain mass ratio of 37.5 was reported by Gonzalez-Buelga *et al.* [36], who tested a commercially realisable device. Here, we will consider the case of a device with a single fixed-inertance inerter which is positioned across the lowest floor and ground levels. Selecting the inertance before optimising the suppression device allows us to scale the device in the same way as is done by selecting the mass ratio for a TMD.

It is known that the vibration suppressors, such as dampers, are installed on braces at different storey levels [37]. The performance of the structures with the brace compliance has been investigated in [38, 39]. In this paper, considering the installation of the vibration absorber, a brace compliance is also included between the structure and the device. Many cost functions could be selected for the optimisation, we select an example one while noting it is the approach proposed in this paper rather than the specific results which is of the most interest. By choosing the relative displacements of the storeys to that of the base as the performance index, the example optimisation objective function is generated. Utilizing the patternsearch and fminsearch functions in MATLAB, the optimum configurations for the suppression device can be obtained. Then making use

of simplification approaches, some approximate optimum configurations with significantly fewer elements are proposed with respect to the inertance and brace stiffness.

This paper is arranged as follows. In Section 2, we introduce an idealised building model, the objective function and the optimisation approach also are presented. Then, in Section 3, we propose a fixed-sized-inerter admittance which is synthesized by seven-element network, named the fixed-sized-inerter layout and the structural response is shown for the optimised device. The simplification of the fixed-sized-inerter configuration is carried out in Section 4 and four simple approximate optimum configurations are identified with respect to the inerter's size and the brace stiffness. Conclusions are drawn in Section 5.

2. BUILDING MODEL AND OBJECTIVE FUNCTION

2.1. Multi-storey building model

The building model is represented by a $n-$storey structure, reduced to a $n-$DOF lumped mass system as shown in Figure 1. The structural damping is taken to be zero because its value is typically small compared with the control device. The vibration suppression device is located between the ground and the first floor, which makes the installation of the absorber much easier and it needs to be noted that only one control system is used at a time. The control system is assumed to be a passive mechanical admittance $Y(s) = F/v$ [17, 40], where F is the force exerted by the control device and v is the relative velocity between the two terminals. Moreover, vibration suppressors, such as dampers, are usually installed via a brace between storey levels. Hence, it is necessary to consider a brace stiffness k_s which is in series with the absorber attached to the first floor. In our research, we consider a three-storey building model with equivalent floor storey masses m and equivalent inter-storey elasticity k. We fix the parameters of the three storey building model as $m = 1\,\mathrm{kNs^2/m}$ and $k = 1500\,\mathrm{kN/m}$. The parameters for the building model are the same as the one used in the TID paper [27] and these numerical values were selected for convenience while retaining realistic natural frequencies and noting that the parameters scale linearly. To include the effect of the brace stiffness, we consider the range $k_s \in [k/10, \infty]$.
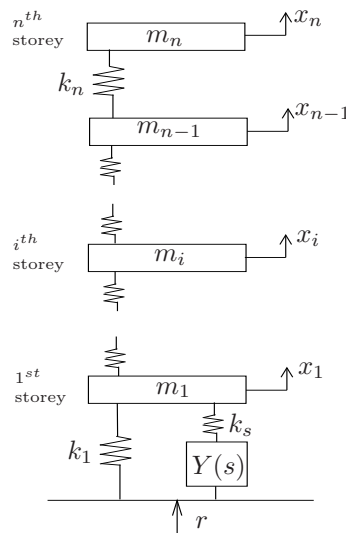

Figure 1. Schematic representation of an idealised building and lower floor suppression device with brace compliance subjected to ground motion.

Defining the variable matrix

$$x = \begin{bmatrix} x_1 & x_2 & x_3 \end{bmatrix}^T$$

where x_i is the displacement of the ith storey and the relative displacement of the ith storey to the base is $z_i = x_i - r$. Then making Laplace transformation of z_i, we can obtain that $Z_i(s) = X_i(s) - R$, hence the steady-state equation of motion for the controlled model of Figure 1, in matrix form, in the Laplace domain is

$$
\begin{bmatrix} m & 0 & 0 \\ 0 & m & 0 \\ 0 & 0 & m \end{bmatrix} s^2 Z + \begin{bmatrix} 2k + \frac{sk_sY(s)}{sY(s)+k_s} & -k & 0 \\ -k & 2k & -k \\ 0 & -k & k \end{bmatrix} Z = - \begin{bmatrix} m \\ m \\ m \end{bmatrix} s^2 R
$$

where $Z = X - R$ represents the vector of relative storey displacements in the Laplace domain.

2.2. Objective function and optimisation approach

There are many design criterions for a vibration absorber [41]. In this paper, we consider the displacements of each building storey relative to that of the base. The objective function is defined as

$$
J_\infty = \max \left(\|T_{R \to Z_i}(j\omega)\|_\infty \right), \ i = 1, \cdots, n \tag{1}
$$

where $T_{R \to Z_i}$ denotes the transfer function from R to Z_i, $\|T_{R \to Z_i}(j\omega)\|_\infty$ is the standard H_∞-norm, which represents the maximum magnitude of $T_{R \to Z_i}$ across all frequencies. We note that many objective functions considering different motions, such as inter-storey drift, and weighted frequency distributions can be devised. Here, as the configuration optimisation approach is of primary interest, we just consider this example objective function.
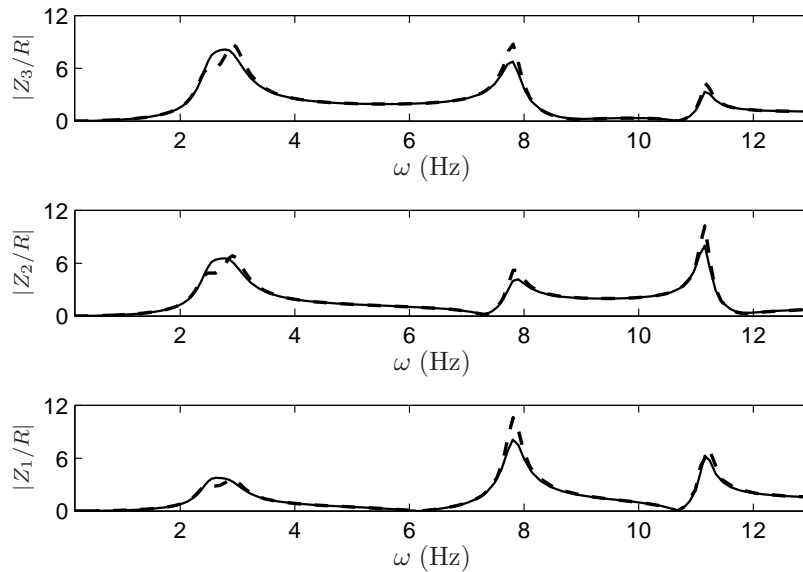

Figure 2. Displacement comparison: optimised TID using (1) with $k_d = 142.7\,\text{kN/m}$, $c_d = 3.263\,\text{kNs/m}$ (thin solid line) and TID proposed in [27] with $k_d = 138.6\,\text{kN/m}$, $c_d = 2.5\,\text{kNs/m}$ (thick dashed line).

The design of the absorber for the MIMO structures is often carried out in the fundamental mode, with initial tuning based on the assumption that the natural frequencies are well separated, hence the contributions from higher mode are ignored. In reality, the modal cross coupling has a deleterious effect on the tuning in some cases. Hence, we propose objective function (1) to avert this problem. In order to show the feasibility of our objective function, we optimise the building model used in [27] with the same TID configuration. The value of the inerter $b = 499\,\text{kg}$ is fixed as the same as that in [27]. By optimising J_∞, we obtain that $k_d = 142.7\,\text{kN/m}$, $c_d = 3.263\,\text{kNs/m}$. The authors of [27] chose the value of spring and damper as $k_d = 138.6\,\text{kN/m}$, $c_d = 2.5\,\text{kNs/m}$ based on Den Hartog tuning method [4] targeting the first mode. By analysing the displacement response with the
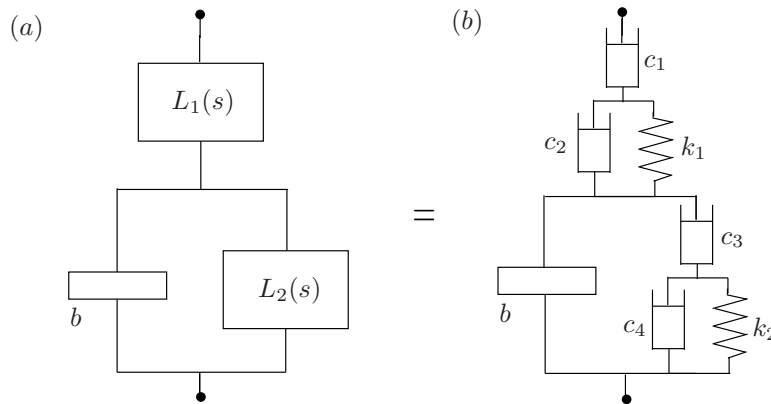
Figure 3. Fixed-sized-inerter layout (a) and corresponding network configuration (b)

TID of these two different set of values, Figure 2 suggests that with objective function (1), the TID device results in much smaller displacements of all the three floors in the vicinity of the second and third fundamental frequencies. Although the displacement of the first storey in the first fundamental frequency obtained from the objective function J_∞ is slightly bigger, the max response displacement of the first fundamental frequency is smaller (for the third storey) comparing with the results in [27].

Using the objective function (1), we compare the TID configuration as an example, with the conventional TMD. Because the inerter device can achieve a higher inertance with a much lower mass via the gearing mechanism [16], we choose the mass of TMD as 100 kg, and the inertance of TID is 1000 kg. By optimising the objective function, we obtain that for the TMD, $J_\infty = 35.45$ with $c_d = 2.51$ kNs/m and $k_d = 32.6$ kN/m, and the TID achieves an optimal value of $J_\infty = 5.03$ with $c_d = 8.08$ kNs/m and $k_d = 290.7$ kN/m.

3. FIXED-SIZED-INERTER (FSI) LAYOUT AND OPTIMISATION RESULTS

In this section, a fixed-sized-inerter layout is introduced. Using network synthesis, it can be realised by a seven-element network comprising of dampers, springs and one inerter. An example of synthesis process is now provided and the optimisation results with this layout for three different brace stiffness versus the inertance will also be shown.

3.1. Network synthesis and fixed-sized-inerter layout

Given a general admittance $Y(s)$ for the mechanical absorber with unknown parameters, the optimum admittance can be obtained by optimising the objective function in MATLAB. As discussed in the introduction, we consider a single fixed size inerter and propose the overall device layout shown in Figure 3(a), named as fixed-sized-inerter layout (FSI layout), where

$$L_1(s) = \frac{s + \alpha_0}{\beta_1 s + \beta_0},$$

$$L_2(s) = \frac{s + \gamma_0}{\delta_1 s + \delta_0}.$$

The admittance of the absorber $Y(s)$ for the layout shown in Figure 3(a) can be expressed as

$$Y(s) = \frac{L_1(s)(bs + L_2(s))}{bs + L_1(s) + L_2(s)}, \tag{2}$$

where we take $b \in [100\,\text{kg}, 3000\,\text{kg}]$.

In the network synthesis, there is a procedure to remove imaginary poles and zeros and subtract positive constants, which is called "Foster Preamble" [42,43]. Using such procedure, it can be shown
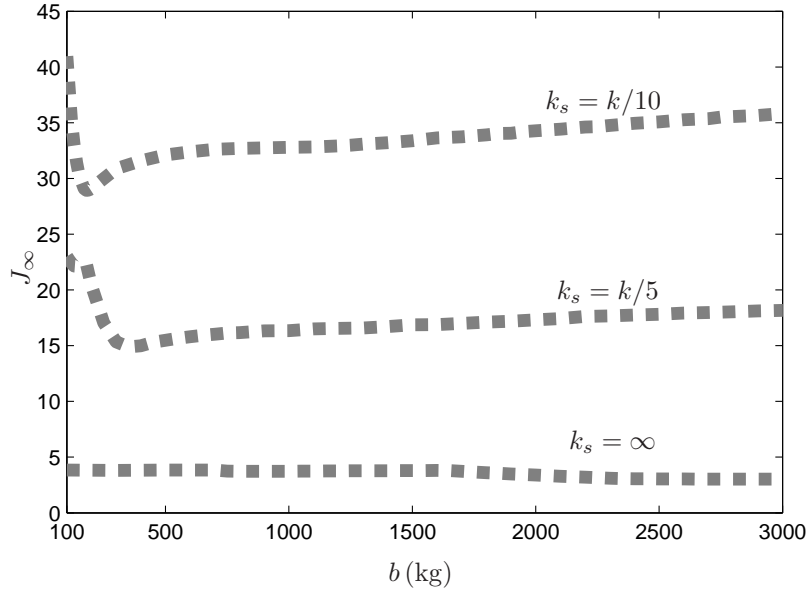
Figure 4. The optimum values of J_∞ with the FSI layout for the three brace stiffness versus b.

that to guarantee $L_1(s)$ and $L_2(s)$ can be realised with spring(s) and damper(s) only, α_0, β_0, β_1, γ_0, δ_0, and δ_1 should be non-negative and satisfy the following two conditions,

$$\beta_0 - \beta_1\alpha_0 \leq 0, \tag{3}$$

and

$$\delta_0 - \delta_1\gamma_0 \leq 0. \tag{4}$$

Based on network synthesis theory, the admittance $Y(s)$ (2) with the conditions (3) and (4) can always be realised by the seven-element network shown in Figure 3(b). The element values of the network of Figure 3(b) can then be obtained. For example, for the case $k_s = \infty$ and $b = 2200\,\mathrm{kg}$, we obtain the optimum parameters of $Y(s)$ as $\alpha_0 = 19.1$, $\beta_1 = 3.35 \times 10^{-5}$, $\beta_0 = 1.00 \times 10^{-11}$ and $\gamma_0 = 1.01 \times 10^3$, $\delta_1 = 27.5$, $\delta_2 = 1.26 \times 10^{-16}$ and it achieves the value of $J_\infty = 3.197$. By using Foster preamble procedure, we can obtain the element values of the seven-element network of Figure 3(b) as: $c_1 = 1.91 \times 10^9\,\mathrm{kNs/m}$, $c_2 = 29.9\,\mathrm{kNs/m}$, $k_1 = 571\,\mathrm{kN/m}$, $c_3 = 8.35 \times 10^{15}\,\mathrm{kNs/m}$, $c_4 = 3.60 \times 10^{-5}\,\mathrm{kNs/m}$ and $k_2 = 3.85 \times 10^{-2}\,\mathrm{kN/m}$. It can then be checked that

$$L_1(s) = \frac{s + \alpha_0}{\beta_1 s + \beta_0} = \frac{c_1(c_2 s + k_1)}{(c_1 + c_2)s + k_1},$$

$$L_2(s) = \frac{s + \gamma_0}{\delta_1 s + \delta_0} = \frac{c_3(c_4 s + k_2)}{(c_3 + c_4)s + k_2}.$$

3.2. Optimisation results for fixed-sized-inerter layout

We now use the FSI layout shown in Figure 3(a) as the candidate vibration suppression device for optimisation. The brace stiffness k_s is chosen from our considered range $k_s \in [k/10, \infty]$. Two boundaries and the median of the range are chosen as the specific brace stiffness to be studied, which are $k_s = \infty$, $k_s = k/5$ and $k_s = k/10$ respectively. Making use of patternsearch and fminsearch command in MATLAB, the optimum results of the objective function (1) for the three different brace stiffness have been shown as the grey dashed line in Figure 4, with respect to the certain range $b \in [100\,\mathrm{kg}, 3000\,\mathrm{kg}]$. It can be seen that the optimum result increases, in terms of the cost function, as the brace stiffness decrease, which reflect the fact that with a less stiff brace a smaller
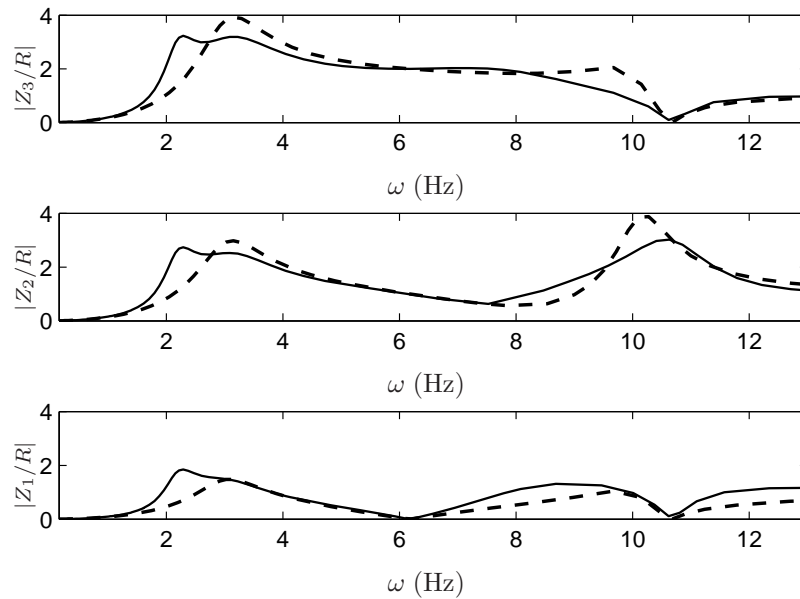
Figure 5. Displacement response comparison: FSI layout (thin solid) when $b = 2200\,\text{kg}$ and damper (thick dashed) for the case $k_s = \infty$.

proportion of the relative displacement between the floors is transmitted to the device, and the fixed brace stiffness $k_s = \infty$ is the most desirable case.

When investigating the proposed FSI layout, it is benefit to consider whether it gives improved level of performance comparing with the commonly used two-terminal device, a viscous damper. An example is presented in Figure 5 to demonstrate that the proposed layout can reduce J_∞ (1) further than a damper. The building model is considered with brace stiffness $k_s = \infty$. The damper $Y(s) = c$ achieves an optimal value of $J_\infty = 3.93$ for $c = 69.94\,\text{kNs/m}$. As discussed in Section 3.1, when $b = 2200\,\text{kg}$, the FSI layout achieves $J_\infty = 3.197$. Here, a 18.7% improvement of the value of J_∞ can be obtained with the FSI layout compared with that of the damper. It can also be seen from Figure 5 that in the first fundamental frequency, the max relative displacement response occurs at third floor and the displacement with the FSI layout is smaller than that with a viscous damper.

4. SIMPLIFICATION OF BENEFICIAL FSI LAYOUT

4.1. Simplification of FSI to IPD and TTID

The FSI configuration shown in Figure 3(b) consists of seven elements and three additional degrees of freedom. It would be complex to implement as a mechanical device. We therefore adopt a simplification approach, where we neglect the parallel elements with a relative small value and replace the series element of a relative large value with a rigid connection. As an example of this process, we consider the case $k_s = \infty$ and $b = 2200\,\text{kg}$, which has been used as example in Section 3.1. A simpler configuration may be achieved by rigidly fixing c_3 (as $c_3 \gg c_4$) and c_1 (as $c_1 \gg c_2$) and neglecting c_4 (as $c_4 \ll c_2$). This simpler configuration, termed the turned TID (TTID, the additional T indicating an additional tuning from spring k_2)) is shown in Figure 6(b_2) and once reoptimised results in the J_∞ of 3.199. There is just 0.3% degradation in J_∞ with this much simpler structure. A comparison of these two systems is given in Figure 7, the response is very close to each other. Following the similar simplification approach for all the range of inertance b and allowing up to 10% degradation of the value of J_∞, the FSI layout can be reduced to two simpler configurations, the TTID and the IPD (inerter in parallel with a damper), shown in Figure 6, for all the three brace
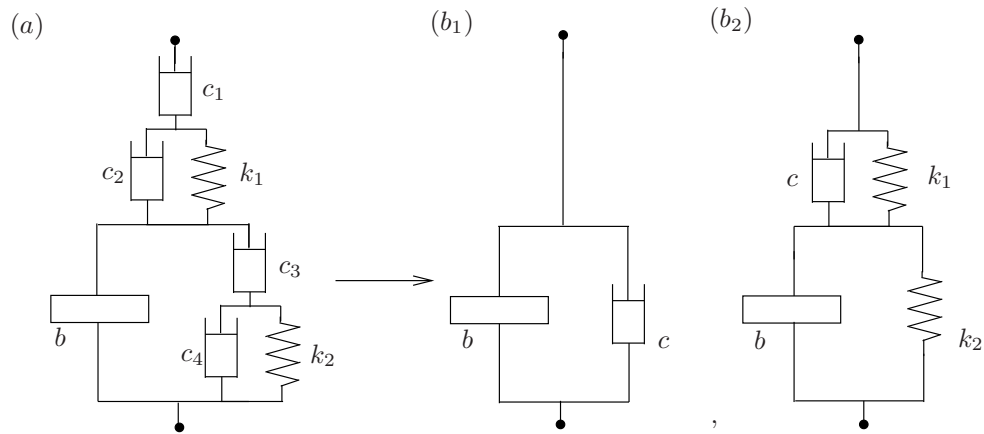
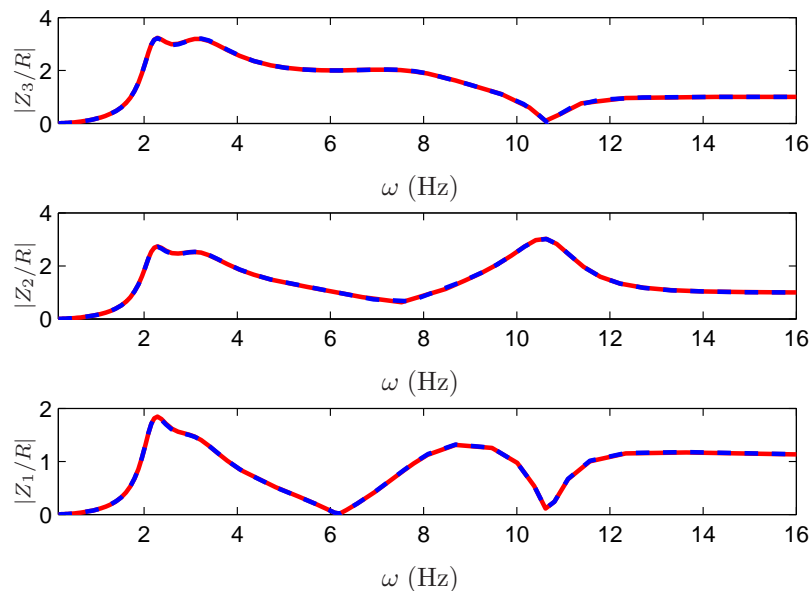Figure 6. (a) The FSI configuration and its simplification to (b_1) the IPD and (b_2) the TTID configurations.

Figure 7. Displacement response comparison: FSI configuration of Figure 6(a) (red solid) and TTID of Figure 6(b_2) (blue dashed) when $b = 2200\,\text{kg}$ and $k_s = \infty$.

stiffness considered. It should be noted that in choosing a 10% degradation in the level of the cost function, we take the view that a 10% improvement in J_∞ does not justify the extra complexity of the absorber configuration along with identically unrealistic element values that are needed to obtain this improvement. Figure 8 shows the optimum values of the objective function J_∞ with the FSI layout, the IPD and the TTID, respectively, when b is in the range of $100\,(\text{kg})$ to $3000\,(\text{kg})$ for the three brace stiffness. Here, the TTID and IPD responses have been truncated in the range of b to show just the regions where they achieve acceptable J_∞ compared with that of the FSI configuration. Short vertical lines show the transition point between the IPD and the TTID. Noted that the IPD and TTID configurations together can provide similar behaviour to the FSI layout with the full range of inerter values considered. For the case $k_s = k/5$, when $b \in [150\,\text{kg}, \ 170\,\text{kg}]$, there appears a highest degradation of J_∞, and it can be checked that 8.3% degradation in J_∞ is the highest with $b = 165\,\text{kg}$, which is below our limitation 10%. Also note that the range covered by the IPD decreases as the brace stiffness k_s decreasing. And when $k_s = k/10$, the FSI structure can be reduced to only one simple structure, the TTID, for the whole range of inertance considered.
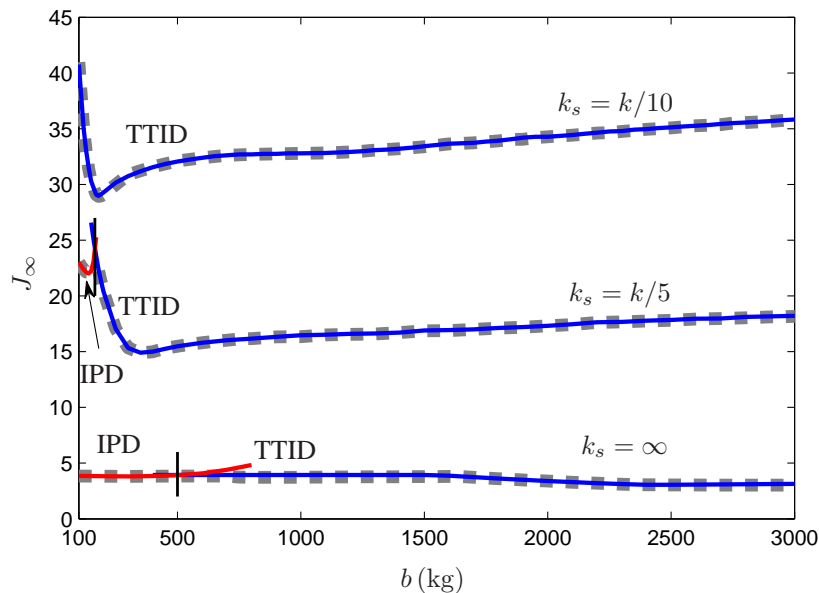
Figure 8. The optimum results comparison between the two simper configurations (IPD with red line, TTID with blue line) and the fixed-size inerter admittance (2) with the FSI layout shown as a grey dashed line.
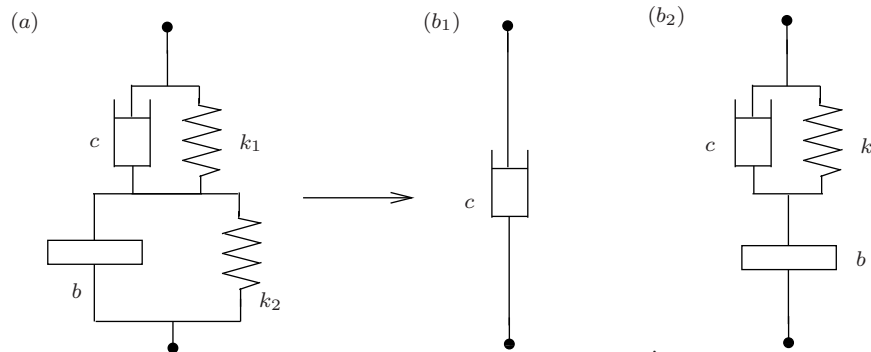

Figure 9. (a) The TTID configuration and its simplification to (b_1) the damper (D) and (b_2) the TID configurations.

4.2. Further Simplification of TTID to TID and Damper

The TTID configuration contains four elements and it is more complicated than the TID [27] and the TVMD [29] mentioned in the introduction since both of them just have three elements. From the optimal elements values obtained for the TTID, it can be noticed that for a range of b value, the TTID can be further reduced to a damper (D) or a TID, shown in Figure 9, using the simplification approach described in Section 4.1. The acceptable degradation of J_∞ for reducing TTID to D and TID configurations was set to 3%. To demonstrate this simplification, we consider the same example used in Section 4.1 with $k_s = \infty$ and $b = 2200$ kg. It has been shown that the FSI layout can be reduced to a TTID, which achieves the value of $J_\infty = 3.199$ with the element values $c = 29.6$ kNs/m, $k_1 = 573.06$ kNs/m and $k_2 = 0.10$ kNs/m. By removing the small spring k_2, the TTID is simplified to a TID. Reoptimising with the TID results in $J_\infty = 3.201$ with $c = 29.6$ kNs/m and $k_1 = 575.95$ kNs/m. The value of J_∞ only increases by 0.06%, which is negligible.

As a result, four simple configurations (IPD, D, TID and TTID) are obtained. It can be seen that the IPD is the special case of the TVMD, which is obtained by adding a spring in series with the IPD. Adding such a series spring to the IPD is similar to including the effect of the brace
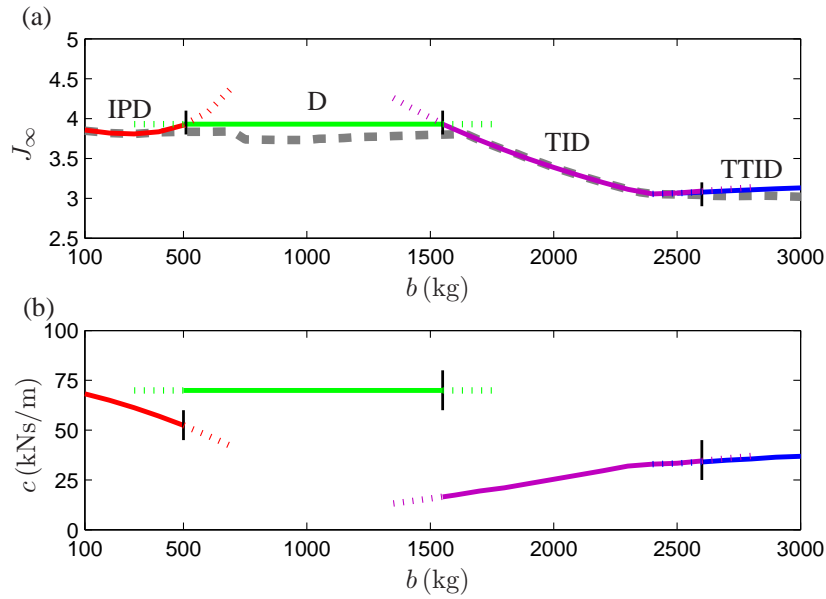
Figure 10. For brace stiffness $k_s = \infty$: (a) the optimum results, (b) the corresponding damping values with IPD (red), Damper (green), TID (purple) and TTID (blue).
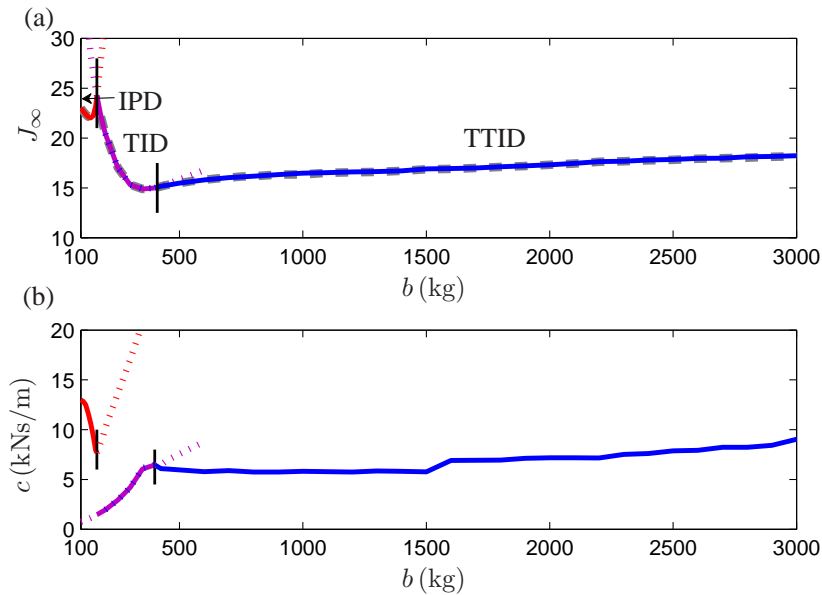

Figure 11. For brace stiffness $k_s = k/5$: (a) the optimum results, (b) the corresponding damping values with IPD (red), TID (purple) and TTID (blue).

stiffness. We note that Ikago *et al.* proposed the TVMD and applied in a different manner with that is considered here, namely it was installed at every story [30]. A comparison of the optimum values of J_∞ using these four simplified configurations with that of the FSI layout for the three brace stiffness $k_s = \infty$, $k_s = k/5$ and $k_s = k/10$ are given in Figures 10(a), 11(a) and 12(a), respectively. The corresponding damping values for the configurations are shown in Figures 10(b), 11(b) and 12(b), respectively. Here, we allow a 10% performance degradation relative to the FSI layout, it can be seen that these four simple systems together can approximately achieve the value of J_∞
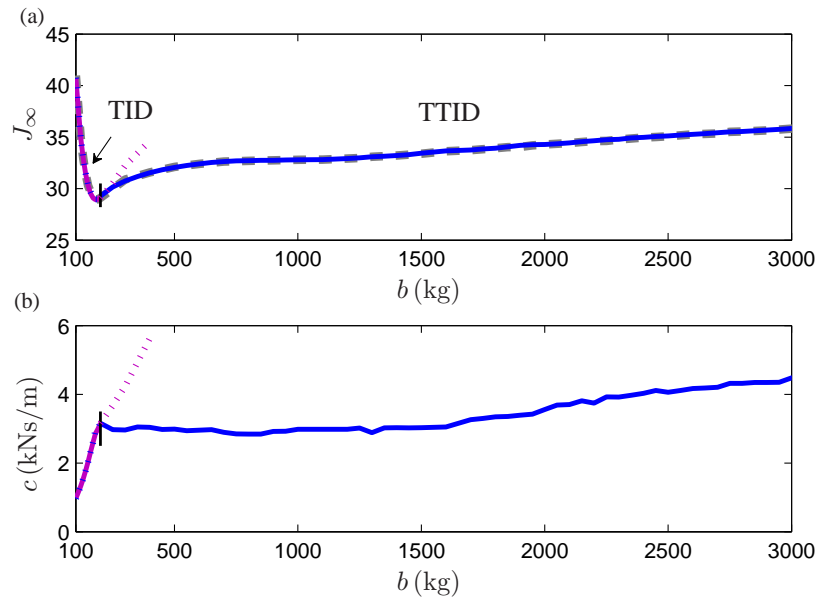
Figure 12. For brace stiffness $k_s = k/10$: (a) the optimum results, (b) the corresponding damping values with TID (purple) and TTID (blue).

of the FSI structure, versus the range of the inerter values considered, while being much easier to implement. Hence, instead of the real optimum configuration (FSI configuration) obtained from the admittance $Y(s)$ (2), these four simple systems are scheduled as the approximate optimum configurations in this paper. Figure 10(a) shows that the approximate optimum structure is an IPD for $k_s = \infty$ when $b \in [100\,\mathrm{kg}, 500\,\mathrm{kg}]$, a single damper when $b \in [500\,\mathrm{kg}, 1550\,\mathrm{kg}]$, a TID when $b \in [1550\,\mathrm{kg}, 2600\,\mathrm{kg}]$ and a TTID when $b \in [2600\,\mathrm{kg}, 3000\,\mathrm{kg}]$. Short vertical lines show the transition point between the four simplified configurations. The dotted lines show the performance of the simplified configurations outside the region in which they outperform the other simple configurations. It can also be noted that the TID and the Damper are simplifications of the TTID, hence the optimum results for the TTID are similar to those of the Damper and the TID in the regions where the TID and Damper are presented as alternative. Recall that the TTID is replaced with the TID or Damper when their cost function values are no more than 3% higher than the TTID, the optimal range of the TTID can be determined. Observe that for $b > 2500\,\mathrm{kg}$, an increase in b leads to an increase in J_∞ (hence worse performance based on the cost function) and an increase in the damping required. This region, which we term the suboptimal region as a larger inerter device requires a larger damper and achieves a worse performance, will be further discussed in Section 4.3. Finally we note that the damper parameter is much lower in the TID than when a pure damper is considered in their optimal regions. As discussed earlier, in the paper by Lazar *et al.* [27] the case where $b = 499\,\mathrm{kg}$ was considered. They proposed the use of the TID. In doing so, they considered the size of a damper that could match the performance of the TID finding that the damping parameter was an order of magnitude larger in the pure damper configuration. Here, instead, the emphasis is on the cost function performance and we find that when optimised the damper can outperform the TID in this region.

The results in Figure 11(a), suggest that for the brace stiffness $k_s = k/5$, only three simple configurations are needed to obtain the similar optimum results, which are the IPD when $b \in [100\,\mathrm{kg}, 165\,\mathrm{kg}]$, the TID when $b \in [165\,\mathrm{kg}, 410\,\mathrm{kg}]$ and the TTID when $b \in [410\,\mathrm{kg}, 3000\,\mathrm{kg}]$. It can be also noted from Figure 11(a) and (b) that for $b > 350\,\mathrm{kg}$, the value of the cost function and the corresponding damping values are increasing as the value of b increasing.

For the case where the brace stiffness $k_s = k/10$, Figure 12(a) shows that the TID and TTID are the approximate optimum configurations when $b \in [100\,\mathrm{kg}, 210\,\mathrm{kg}]$ and $b \in [210\,\mathrm{kg}, 3000\,\mathrm{kg}]$
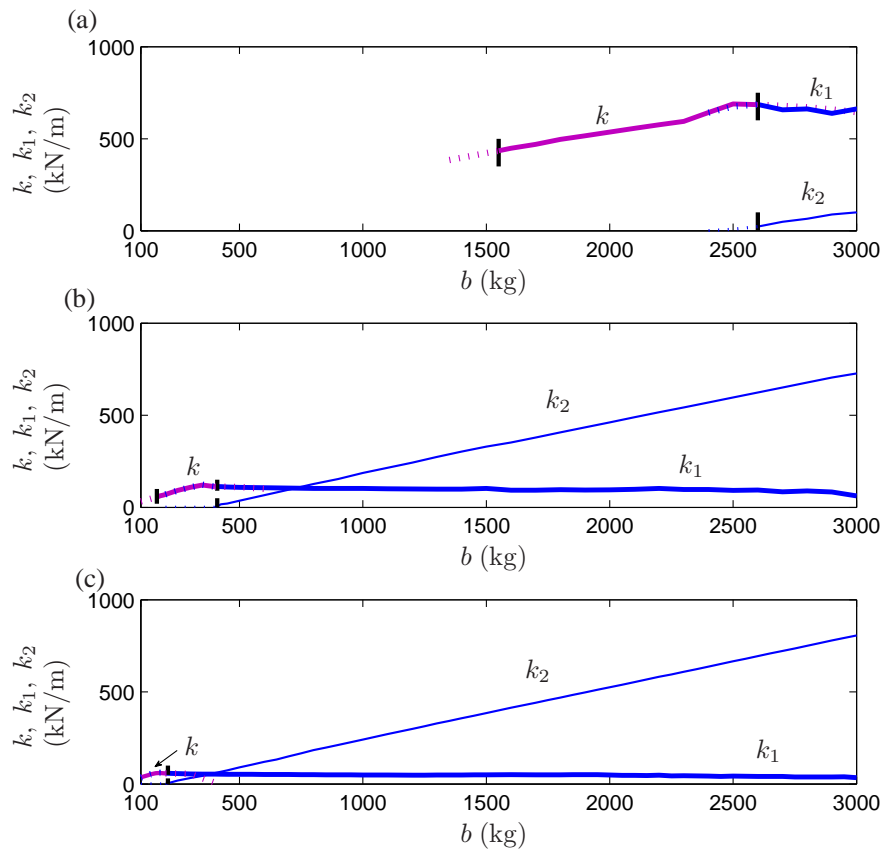
Figure 13. The corresponding spring values of the TID (thick purple) and the TTID (thick blue for k_1, thin blue for k_2) for (a) $k_s = \infty$, (b) $k_s = k/5$ and (c) $k_s = k/10$.

respectively. Furthermore, in conjunction with the corresponding damping values shown in Figure 12(b), it can be seen that the optimum value of J_∞ and the corresponding damping values become larger with the value of b increasing for the range of $b > 180$ kg. As a result, the region that $b > 180$ kg is suboptimal when brace stiffness $k_s = k/10$.

Figure 13 shows the corresponding values for the stiffness of the TID and the TTID for the three different brace stiffness $k_s = \infty$, $k_s = k/5$ and $k_s = k/10$ with respect to the inerter's size within which the TID or the TTID configuration is optimum.

The optimal configurations within the range of $b \in [100\,\text{kg}, 3000\,\text{kg}]$ and the corresponding parameters have been summarised in Table I for three different brace stiffness. It can be seen that the configuration TID is the optimal configuration for all the three brace stiffness $k_s = \infty$, $k_s = k/5$ and $k_s = k/10$. The optimum value of J_∞ increase and the optimum parameters of TID become smaller as the brace stiffness decreasing.

4.3. Proposed simple configurations

From the analysis shown above, we can conclude that these four simple configurations are effective in replacing the FSI layout as they provide a similar value of J_∞ for the base excited structure. What is more, the approximate optimum simple configuration is different for the different b value and different brace stiffness k_s. Also a larger inerter does not always give a better performance, but a larger brace stiffness can provide a smaller value of J_∞.

Based on the conclusions obtained for the three specific brace stiffness $k_s = \infty$, $k_s = k/5$ and $k_s = k/10$, we optimise the objective function with these four simple configurations (IPD, D, TID

Table I. The optimal configurations for $b \in [100\,\text{kg}, 3000\,\text{kg}]$ for the three different brace stiffness.

Brace stiffness	Optimal configurations				
	Type	J_∞	$b\,(\text{kg})$	$c\,(\text{kNs/m})$	$k\,(\text{kN/m})$
$k_s = \infty$	TID	3.05	2400	32.9	642.3
$k_s = k/5$	TID	14.88	350	6.05	121.3
$k_s = k/10$	TID	28.93	180	2.85	59.4

and TTID) for many brace stiffness k_s values in the range of $[k_1/10, \infty]$. The optimal regions for these four simple configurations with respect to the b value and structured to brace stiffness ratio k/k_s are shown in Figure 14.

This provides guidance for selecting the appropriate configurations given a certain inertance and brace stiffness values. By identifying the region, in which increasing b always give a larger minimum value of J_∞ and at the same time there is no meaningful reduction in the damper parameter, the boundary of the suboptimal region is identified and it is shown as a shaded region limited by a black dashed line with circle markers in Figure 14.
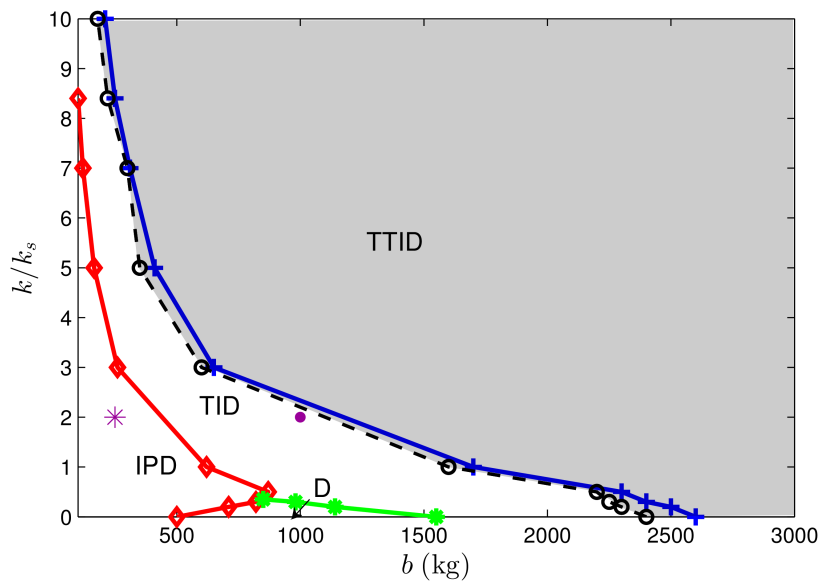
Figure 14. The optimum structures with different b values and brace stiffness ratio k/k_s.

Finally, we consider the performance of the building model subjected to earthquake base excitation. In line with the TID paper by Laser *et al.* [27], we chose a ground acceleration recorded from the Tohoku earthquake that took place in Japan on the 11th of March, 2011, which is shown in Figure 15(a). All the structural parameters are kept unchanged, the optimum control system is selected based on the inertance value and the brace stiffness k_s. Selecting $b = 250\,\text{kg}$ and $k_s = k/2$ (shown as the asterisk in Figure 14), the approximate optimum control configuration is the IPD. By optimising the objective function (1), the optimal parameters for the IPD can be obtained as $c = 25.6\,\text{kNs/m}$. The optimum relative displacement time history of the third floor is shown as the red line of Figure 15(b).
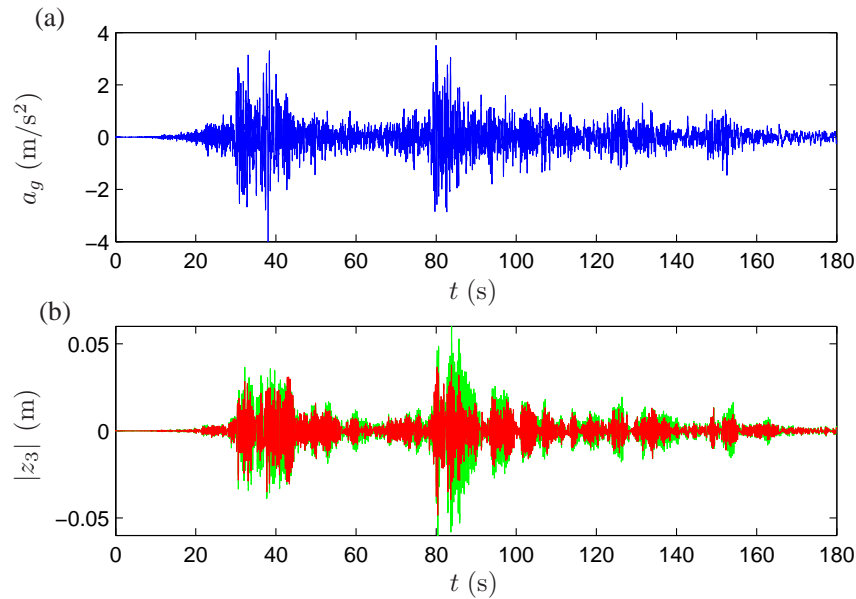
Figure 15. (a) Ground acceleration time-history and (b) 3rd floor relative displacement time history with optimum IPD configuration (red) and optimum TID configuration (green) for $b = 250\,\text{kg}$ and $k_s = k/2$.
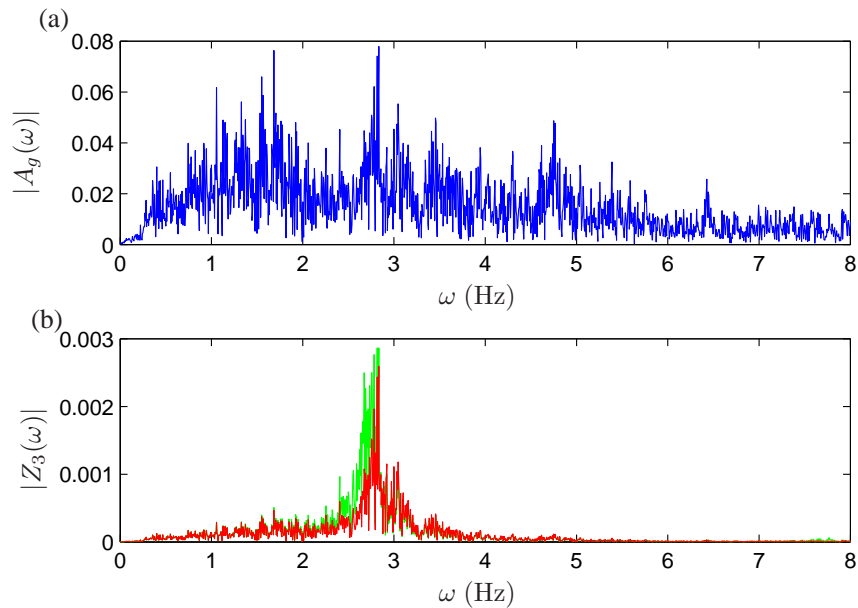

Figure 16. Single-sided Fourier spectra of (a) the ground acceleration and (b) the 3rd floor relative displacement with optimum IPD configuration (red) and optimum TID configuration (green) for $b = 250\,\text{kg}$ and $k_s = k/2$.

By optimising the model with the TID for the same $b = 250\,\text{kg}$ and $k_s = k/2$, we obtain the optimal spring value $k = 81.3\,\text{kN/m}$ and the damping value $c = 1.94\,\text{kNs/m}$. The corresponding relative displacement time history of the third floor is shown as the green line of Figure 15(b). It can be noted that the IPD perform better than the TID at this point in b, k/k_s space, as expected from Figure 14. Figure 16 shows the single-sided Fourier spectrum of the ground acceleration and the third floor relative displacement response of the optimum IPD and TID configurations. The

highest amplitudes are attained at low frequencies, and therefore only the $0 - 8$ Hz frequency range is shown. The first natural frequency of the structure is $\omega_1 = 2.74$ Hz, tuned to match the high amplitude frequency region of the chosen ground motion. The Fourier spectra of Figure 16(b) reflects the performance improvement compared the IPD configuration with the TID configuration as obtained in Figure 15.
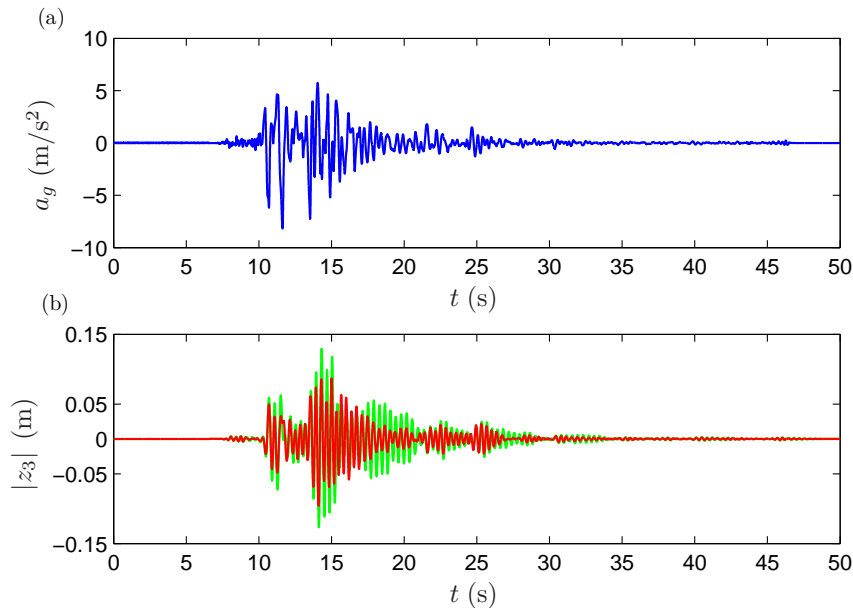

Figure 17. (a) Ground acceleration time-history and (b) 3rd floor relative displacement time history with optimum IPD configuration (red) and optimum TID configuration (green) for $b = 250$ kg and $k_s = k/2$.
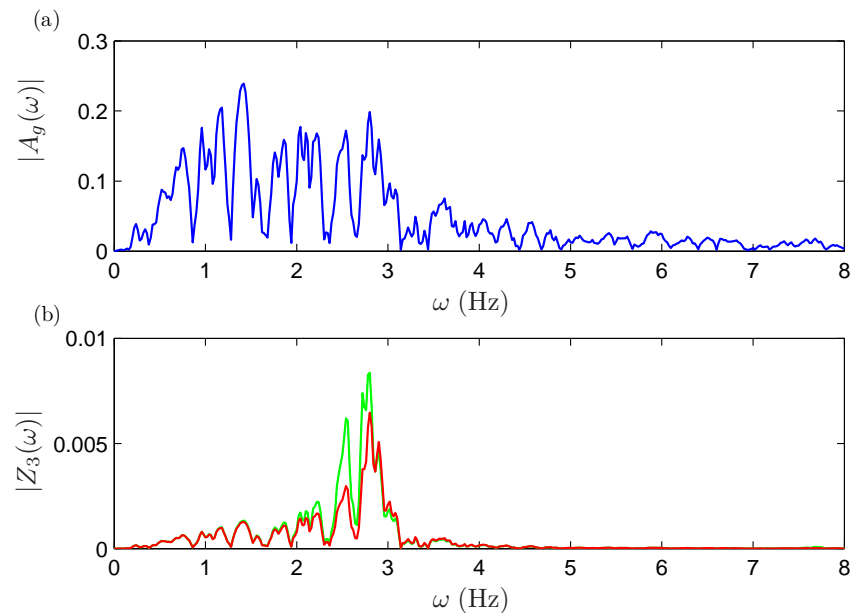

Figure 18. Single-sided Fourier spectra of (a) the ground acceleration and (b) the 3rd floor relative displacement with optimum IPD configuration (red) and optimum TID configuration (green) for $b = 250$ kg and $k_s = k/2$.
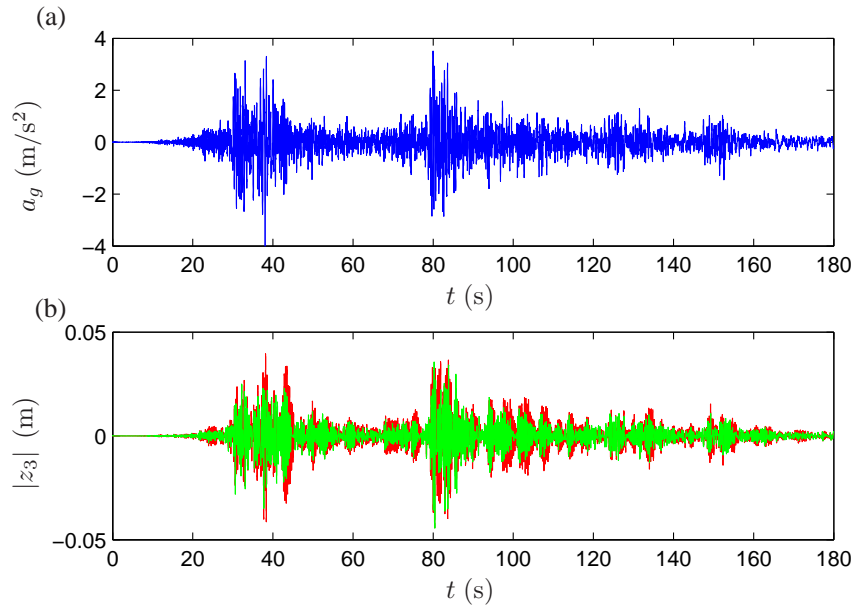
Figure 19. (a) Ground acceleration time-history and (b) 3rd floor relative displacement time history with IPD configuration (red) and TID configuration (green) for $b = 1000\,\text{kg}$ and $k_s = k/2$.
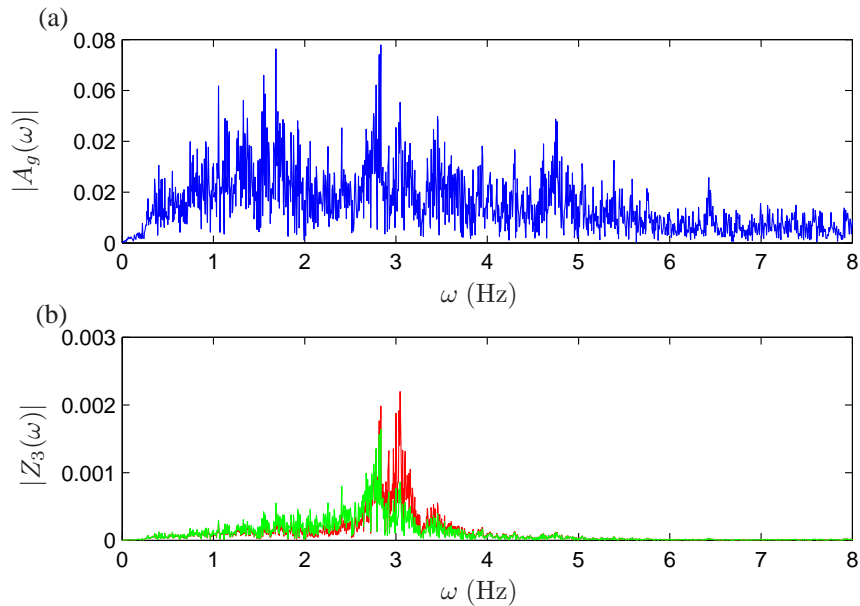

Figure 20. Single-sided Fourier spectra of (a) the ground acceleration and (b) the 3rd floor relative displacement with IPD configuration (red) and TID configuration (green) for $b = 1000\,\text{kg}$ and $k_s = k/2$.

The proposed configuration is also tested on a shorter duration recorded from Kobe, 1995. The time history and the single-sided Fourier spectrum are shown in Figure 17(a) and Figure 18(a). The relative displacement time history and the single-sided Fourier spectrum of the third floor with the TID (IPD) have been shown as the green line (red line) of Figure 17(b) and Figure 18(b), respectively. Again it can be seen that the IPD performs better than the TID when $k_s = k/2$ and $b = 250\,\text{kg}$.

Choosing the value of inerter and brace stiffness as $b = 1000 \, \mathrm{kg}$, $k_s = k/2$ (shown as the dot in Figure 14), the approximate optimum control configuration is the TID according to Figure 14. Comparing with the optimum IPD configuration, Figure 19(b) and Figure 20(b) both show the optimum performance of the TID is better than that of the IPD in the time domain and frequency domain respectively, as expected.

5. CONCLUSIONS

This paper proposed four optimum linear passive absorber configurations with one inerter for a building model with respect to the inerter's size and the brace stiffness. First, a generalised building model was introduced and a steady-state equation of motion for a controlled three-storey model with the brace stiffness has been derived. Then, we introduced a fixed-sized-inerter layout for the suppression device considering of the manufacture problem in reality. Making use of the network synthesis theory, the corresponding fixed-sized-inerter configuration has been obtained. Optimisation results of this fixed-sized-inerter (FSI) layout have been given as a function of the inerter's size for the three different brace stiffness. Since the FSI configuration has seven elements and three additional degrees of freedom, a simplification process has been carried out. As a result, four simplified optimum configurations for the suppression device have been obtained with respect to the different inerter's size and different brace stiffness. The corresponding parameter values for these optimum configurations have also been presented. Finally, the responses to the Tohoku earthquake data were presented to show the validity of the proposed optimal configurations.

REFERENCES

1. Frahm H. Device for damping vibrations of bodies 1909.
2. Villaverde R. Reduction in seismic response with heavily-damped vibration absorbers. *Earthquake Engineering and Structure Dynamics* 1985; **13**:33–42.
3. Sadek F, Mohraz B, Taylor AW, Chung RM. A method of estimating the parameters of tuned mass damper for seismic applications. *Earthquake Engineering and Structure Dynamics* 1997; **26**:617–635.
4. Den Hartog JP. *Mechanical Vibration*. McGraw Hill: York, PA, USA, 1940.
5. Fujino Y, Abe M. Design formulas for tuned mass dampers based on a perturbation technique. *Earquake Engineering and Structural Dynamics* 1993; **22**:833–854.
6. Moutinho C. An alternative methodology for designing tuned mass dampers to reduce seismic vibrations in building structures. *Earthquake Engineering and Structural Dynamics* 2012; **41**:2059–2073.
7. Angelis MD, Perno S, Reggio A. Dynamic response and optimal design of structures with large mass ratio TMD. *Earthquake Engineering and Structural Dynamics* 2012; **41**:41–60.
8. Anh ND, Nguyen NX. Extension of equivalent linearization method to design of TMD for linear damped systems. *Structural Control and Health Monitoring* 2012; **19**:565–573.
9. Krenk S. Frequency analysis of the tuned mass damper. *Journal of Applied Mechanics* 2005; **72**:936–942.
10. Yang F, Sedaghati R, Esmailzadeh E. Optimal design of distributed tuned mass dampers for passive vibration control of structures. *Structural Control and Health Monitoring* 2015; **22**(2):221–236.
11. Casciati F, Giuliano F. Performance of multi-TMD in the towers of suspension bridges, journal of vibration and control. *Journal of Vibration and Control* 2009; **15**(6):821–847.
12. Xiang P, Nishitani A. Optimum design for more effective tuned mass damper system and its application to base-isolated buildings. *Structural Control and Health Monitoring* 2014; **21**(1):98–114.
13. Soong TT, Dargush GF. *Passive energy dissipation systems in structural engineering*. John Wiley & Sons: Chichester, West Sussex, England, 1997.
14. Miyamoto HK, Gilani ASJ, Garza J, Mahin SA. *Seismic retrofit of a landmark structure using a mass damper*. Improving the Seismic Performance of Existing Buildings and Other Structures 2009.
15. Tributsch A, Adam C. Evaluation and analytical approximation of tuned mass damper performance in an earthquake environment. *Smart Structures and Systems* 2012; **10**(2):155–179.
16. Smith MC. Synthesis of mechanical networks: the inerter. *IEEE Transactions on Automatic Control* 2002; **47**(10):1648–1662.

17. Papageorgiou C, Smith MC. Positive real synthesis using matrix inequalities for mechanical networks: application to vehicle suspension. *IEEE Transactions on Control Systems Technology* 2006; **14**(3):423–435.

18. Smith MC, Wang FC. Performance benefits in passive vehicle suspensions employing inerters. *Vehicle System Dynamics* 2004; **42**:235–237.

19. Smith MC. http://www.eng.cam.ac.uk/news/stories/2008/mclaren [19 August,2008].

20. Evangelou S, Limebeer DJN, Sharp RS, Smith MC. Mechanical steering compensation for high-performance motorcycles. *Journal of Applied Mechanics* 2007; **74**:332–346.

21. Evangelou S, Limebeer DJN, Sharp RS, Smith MC. Control of motorcycle steering instabilities - passive mechanical compensators incorporating inerters. *IEEE Control Systems Magazine* 2006; **26**(5):78–88.

22. Jiang JZ, Smith MC, Houghton NE. Experimental testing and modelling of a mechanical steering compensator. *The 3rd International Symposium on Communications, Control and Signal Processing (ISCCSP)*, 2007; 249–254.

23. Wang FC, Liao MK, Liao BH, Su WJ, Chan HA. The performance improvements of train suspension systems with mechanical networks employing inerters. *Vehicle System Dynamics* 2009; **47**(7):805–830.

24. Jiang JZ, Matamoros-Sanchez AZ, Goodall RM, Smith MC. Passive suspensions incorporating inerters for railway vehicles. *Vehicle System Dynamics:International Journal of Vehicle Mechanics and Mobility* 2011; **50**:263–276.

25. Brzeski P, Pavlovskaia E, Kapitaniak T, Perlikowski P. The application of inerter in tuned mass absorber. *International Journal of Non-linear Mechanics* 2015; **70**:20–29.

26. Wang F, Su W, Chen C. Building suspensions with inerters. *Proceedings of the Institution of Mechanical Engineers, Part C, Journal of Mechanical Engineering Science* 2010; **224**:1650–1616.

27. Lazar IF, Neild SA, Wagg DJ. Using an inerter-based device for structural vibration suppression. *Earthquake Engineering and Structure Dynamics* 2014; **43**:1129–1147.

28. Krenk S, Høgsberg J. Tuned resonant mass or inerter-based absorbers: unified calibration with quasi-dynamic flexibility and inertia correction. *Proceedings of the Royal society A* 2016; **472**.

29. Ikago K, Saito K, Inoue N. Seismic control of single-degree-of-freedom structure using tuned viscous mass damper. *Earthquake Engineering and Structure Dynamics* 2012; **41**:453–474.

30. Ikago K, Sugimura Y, Saito K, Inoue N. Seimic displacement control of multiple-degree-of-freedom structures using tuned viscious mass dampers. *Proceedings of the 8th International Conference on Structural Dynamics*, Leuven, Belgium, 2011.

31. Takewaki I, Murakami S, Yoshitomi S, Tsuji M. Fundamental mechanism of earthquake response reduction in building structures with inertial dampers. *Structural Control and Health Monitoring* 2012; **19**:590–608.

32. Marian L, Giaralis A. Optimal design of a novel tuned mass-damper-inerter (TMDI) passive vibration control configuration for stochastically support-excited structural systems. *Probabilistic Engineering Mechanics* 2014; **38**:156–164.

33. Gonzalez-Buelga A, Clare LR, Neild SA, Jiang JZ, Inman DJ. An electromagnetic inerter-based vibration suppression device. *Smart Materials and Structures* 2015; **24**(5).

34. Bott R, Duffin RJ. Impedance synthesis without use of transformers. *Journal of Applied Physics* 1949; **20**:816.

35. Jiang JZ, Smith MC. Regular positive-real functions and five-element network synthesis for electrical and mechanical networks. *IEEE Transactions on Automatic Control* 2011; **56**(6):1275–1290.

36. Gonzalez-Buelga A, Lazar IF, Jiang JZ, Neild SA, Inman DJ. Assessing the effect of nonlinearities on the performance of a tuned inerter damper. *Structural Control and Health Monitoring* ; In press.

37. Niwa N, Kobori T, Takahashi M, Hatadatt T, Kurinott H, Tagami J. Passive seismic response controlled high-rise building with high damping device. *Earthquake Engineering and Structural Dynamics* 1995; **24**:655–671.

38. Bursi OS, Gerstle KH, Sigfusdottir A, Zitur JL. Behavior and analysis of bracing connections for steel frames. *Journal of Constructional Steel Research* 1994; **30**:39–60.

39. Uriz P, Mahin SA. Seismic performance assessment of concentrically braced steel frames. *13th World Conference on Earthquake Engineering*, Vancouver, B.C., Canada, 2004.

40. Shearer JL, Murphy AT, Richardson HH. *Introduction to system dynamics*. Addison-Wesley: USA, 1967.

41. Warburton GB. Optimum absorber parameters for various combinations of response and excitation parameters. *Earthquake Engineering and Structural Dynamics* 1982; **10**:381–401.

42. Valkenburg MEV. *Introduction to Modern Network Synthesis*. John Wiley & Sons, 1960.

43. Storer JE. *Passive Network Synthesis*. McGraw-Hill Book Company, 1957.